RESOLUTION AND STABILITY ANALYSIS IN FULL-APERTURE, LINEARIZED CONDUCTIVITY AND WAVE IMAGING

HABIB AMMARI, JOSSELIN GARNIER, AND KNUT SØLNA

(Communicated by Walter Craig)

ABSTRACT. In this paper we consider resolution estimates in both the linearized conductivity problem and the wave imaging problem. Our purpose is to provide explicit formulas for the resolving power of the measurements in the presence of measurement noise. We show that the low-frequency regime in wave imaging and the inverse conductivity problem are very sensitive to measurement noise, while high frequencies increase stability in wave imaging.

1. INTRODUCTION

The inverse conductivity problem is to find a conductivity inclusion from boundary measurements. This problem lays a mathematical foundation to electrical impedance tomography, which is a method of imaging the interior of a body by measurements of current flows and voltages on its surface. On the surface one prescribes current sources and measures voltage (or vice versa) for some or all positions of these sources. The same mathematical model works in a variety of applications, such as breast cancer imaging and mine detection.

The main objective of this paper is to introduce for the first time the notion of resolution in solving the inverse conductivity problem and precisely quantify some important non-intuitive facts in imaging. Since Rayleigh's work, it has been admitted that the resolution measure in wave imaging is of order half the operating wavelength [11]. This is a quite empirical limit on the resolution and is indeed intriguing if stated independently of the signal-to-noise ratio in the data. Moreover, it has been noted that stability of the inversion increases at high frequency, and infinite resolution can be achieved in the near-field [8, 14, 21]. Furthermore, the link between conductivity and wave imaging has stayed quite mysterious. This paper is an attempt to mathematically explain all of these important observations and researchers' beliefs. In doing so, we perform precise resolution estimates in the case of conductivity data, and we contrast them with resolution estimates based on Helmholtz data. In our analysis we moreover make use of asymptotic characterization of the measurements to get explicit results on their resolving power, i.e., their ability to separate small details. It is known that the inverse problems discussed in this paper are exponentially instable in the general case [23].

For both the conductivity and the wave problems, we linearize the imaging problem and consider the imaging of a perturbed disk. For the conductivity problem, the data are collected on the boundary of a background medium containing the perturbed disk, while for the Helmholtz equation, they consist of multi-static measurements on coincident transmitter and receiver arrays. The Born approximation is used in the wave propagation problem.

For the linearized conductivity problem, we first show that on the one hand, we have "infinite resolution" in the near-field limit and, on the other hand, that the relative resolution decreases rapidly with "depth" (the depth increases when the radius of the inclusion decreases). We also give conditions on the signal-to-noise ratio (SNR) and the radius of the inclusion in order to resolve the pth Fourier mode of the perturbation and explicitly answer the question: for a fixed SNR and radius of the unperturbed disk, which modes can be resolved? We finally characterize the smallest radius one can probe for a certain mode number p and a given SNR and show that the linearized inverse conductivity problem is very sensitive to noise.

For the wave imaging problem under the Born approximation, we consider two regimes: a high-frequency regime where the radius of the inclusion is much larger than the wavelength and a low-frequency regime where it is smaller. We first show that in the high-frequency regime the resolution estimates are relatively insensitive to noise for modes that correspond to lengths larger than half a wavelength. High frequencies increase stability. On the other hand, the low-frequency regime is, as in the conductivity case, very sensitive to noise. We provide explicit formulas for the modes that can be estimated for a given SNR and radius of the inclusion.

In connection with our results, we refer in particular to the recent work by Isakov [21] and the one by Nagayasu-Uhlmann-Wang [24]. For further discussions on resolution for conductivity and wave imaging, see [6, 9, 10, 12, 13, 17, 20]. In [21], a proof of increasing stability in wave imaging when frequency is growing was given. In [24], a stability estimate for a linearized conductivity problem was derived. Our results in this paper confirm these important observations and quantify them precisely in terms of the SNR. As far as we know, our formulas for the resolving power of the measurements in the presence of measurement noise are new. They provide a deep understanding of the ill-posed nature of the considered imaging problems and clarify the connection between the inverse conductivity problems and the wave imaging problems. In the limited-view case, we have very recently performed resolution estimates and described the effect of the limited-view aspect on the resolving power of the noisy measurements [3]. We have in particular shown that, in the shallow probing regime, where the inclusion is close to the boundary of the background medium, we can resolve for any signal-to-noise ratio a sufficiently shallow perimeter perturbation of a conductivity inclusion on the overlap of the source and receiver apertures.

2. Interface estimation with conductivity data

In this section we discuss estimation in the case of conductivity data in the two-dimensional case. We will contrast this process with estimation based on Helmholtz data in Section 3. Our objective is to image inclusions from noisy boundary measurements. The inclusions are with constant material parameters. To simplify this severely ill-posed problem, we consider only changes in the inclusion shapes. The

reconstruction problem is therefore linearized. We discuss the concepts of resolution and stability and perform precise estimates of the resolving power of noisy measurements.

2.1. **Differential measurements.** The measurements are taken on a circle of unit radius in our non-dimensionalized setting. The domain of interest, encapsulated by the measurements, is thus

$$(1) \qquad \Omega = \left\{ \boldsymbol{x} = r\boldsymbol{e}_\theta \mid r \le 1,\, 0 \le \theta < 2\pi \right\},$$

where $\boldsymbol{e}_\theta = (\cos\theta, \sin\theta)$. Imbedded in the domain there is a homogeneous inclusion centered at the origin and with the shape of a perturbed circle. As said before, our objective is to estimate the rim of the inclusion. We denote the domain of the unperturbed disk by D and the perturbed domain by D_ε:

$$(2) \qquad D \;=\; \left\{ \boldsymbol{x} = r\boldsymbol{e}_\theta \mid r \le \alpha,\, 0 \le \theta < 2\pi \right\},$$

$$(3) \qquad D_\varepsilon \;=\; \left\{ \boldsymbol{x} = r\boldsymbol{e}_\theta \mid r \le \alpha + \varepsilon h(\theta),\, 0 \le \theta < 2\pi \right\}.$$

Here we let h be order one and assume that h is of class $\mathcal{C}^1$ and $\varepsilon \ll 1$.

The field for different source configurations is indexed by $m = \pm 1, \pm 2, \cdots$ and is chosen to solve in the perturbed case:

$$(4) \qquad \nabla \cdot (1 + (k-1)\chi_{D_\varepsilon})\nabla u_\varepsilon^m = 0\,, \qquad \boldsymbol{x} \in \Omega\,,$$

with the Neumann boundary conditions at the surface $\partial\Omega$:

$$(5) \qquad \frac{\partial u_\varepsilon^m}{\partial \nu}(\boldsymbol{e}_\theta) = e^{-im\theta}\,, \qquad \theta \in [0, 2\pi)\,, \qquad \int_0^{2\pi} u_\varepsilon^m(\boldsymbol{e}_\theta)d\theta = 0\,.$$

Here, ν denotes the outward normal to $\partial\Omega$, the positive constant k is the contrast in the conductivity between the inclusion and the background, and $f(\boldsymbol{e}_\theta) := f(r = 1, \theta)$. The field corresponding to the *unperturbed* domain D is denoted by $u^m = u_0^m$. The differential measurements are denoted by

$$(6) \qquad \hat{a}_{n,m} = \int_0^{2\pi} e^{-in\theta}(u_\varepsilon^m - u^m)(\boldsymbol{e}_\theta)d\theta\,.$$

A central point of our analysis is to assess the resolving power of the measurements in the presence of measurement or instrument noise. We thus introduce

$$(7) \qquad \hat{a}_{n,m}^{\mathrm{meas}} = \hat{a}_{n,m} + \sigma \hat{W}_{n,m}\,,$$

with the noise terms $\hat{W}_{n,m}$ modeled as independent standard complex circularly symmetric Gaussian random variables (such that $\mathbb{E}[|\hat{W}_{m,n}|^2] = 1$) and σ thus modeling the noise magnitude.

In our analysis we moreover make use of asymptotic characterization of the wave field to get explicit results on the resolving power of the measurements. This representation uses the results of [5]. In fact, for any $|n|, |m| \ll (1/\varepsilon)$, we have the representation

$$(8) \qquad \hat{a}_{n,m} = (\mathcal{Q}\hat{h})_{n,m} + \varepsilon^2 \hat{V}_{n,m}\,,$$

where

$$(9) \qquad (\mathcal{Q}\hat{h})_{n,m} = \varepsilon c_{n,m}(\alpha, k)\hat{h}_{n+m}\,,$$

with the coefficients

$$(10) \qquad c_{n,m}(\alpha, k) = -\frac{8\pi(k - \mathrm{sign}(nm))}{\alpha(k-1)} \frac{1}{(\alpha^{-|n|}\frac{k+1}{k-1} + \alpha^{|n|})(\alpha^{-|m|}\frac{k+1}{k-1} + \alpha^{|m|})}$$

if $nm \neq 0$ and $c_{n,m}(\alpha, k) = 0$ if $nm = 0$. Here we have used the Fourier convention

$$(11) \qquad \hat{h}_p = \frac{1}{2\pi} \int_0^{2\pi} h(\theta)e^{-ip\theta}\,d\theta\,, \qquad h(\theta) = \sum_{p=-\infty}^{\infty} \hat{h}_p e^{ip\theta}\,.$$

Thus, we have

$$(12) \qquad \hat{a}_{n,m}^{\mathrm{meas}} = (\mathcal{Q}\hat{h})_{n,m} + \sigma\hat{W}_{n,m} + \varepsilon^2\hat{V}_{n,m}\,.$$

Note that $(\mathcal{Q}\hat{h})_{n,m} = (\mathcal{Q}\hat{h})_{m,n}$ and $(\mathcal{Q}\hat{h})_{n,-m} = (\mathcal{Q}\hat{h})_{-n,m}$.

2.2. **Short range sharp resolving power of conductivity.** Our objective now is to identify the rim or perimeter perturbation of the inclusion, that is, the function h. Note that, from (8), only $\hat{h}_p$ for $0 < |p| \ll 1/\varepsilon$ can be reconstructed from boundary measurements. Therefore, let $M \ll 1/\varepsilon$ be a positive integer and suppose that $\hat{h}_p = 0$ for $|p| \geq M$.

The adjoint of the operator $\mathcal{Q}$ defined by (9) is

$$(13) \qquad (\mathcal{Q}^\star \hat{a})_p = \varepsilon \sum_{j=-\infty}^{\infty} \overline{c_{p-j,j}(\alpha, k)}\,\hat{a}_{p-j,j}\,.$$

We moreover have

$$(14) \qquad (\mathcal{Q}^\star \mathcal{Q}\hat{h})_p = \varepsilon^2 q_p(\alpha, k)\hat{h}_p\,, \qquad q_p(\alpha, k) = \sum_{j=-\infty}^{\infty} |c_{p-j,j}(\alpha, k)|^2\,.$$

The least squares estimate of $\hat{h}_p$ using $\hat{a}^{\mathrm{meas}}$ is (see, for instance, [15])

$$\begin{aligned} \hat{h}_p^{\mathrm{est}} &= \left((\mathcal{Q}^*\mathcal{Q})^{-1}\mathcal{Q}^*\hat{a}^{\mathrm{meas}}\right)_p = \varepsilon^{-2}q_p(\alpha, k)^{-1}\left(\mathcal{Q}^*\hat{a}^{\mathrm{meas}}\right)_p \\ (15) \qquad &= \hat{h}_p + \varepsilon^{-2}q_p(\alpha, k)^{-1}\left(\mathcal{Q}^*(\sigma\hat{W} + \varepsilon^2\hat{V})\right)_p\,. \end{aligned}$$

We then have

$$(16) \qquad \mathbb{E}\left[|\hat{h}_p^{\mathrm{est}} - \hat{h}_p|^2\right] \leq q_p(\alpha, k)^{-1}\left[\left(\frac{\sigma}{\varepsilon}\right)^2 + \varepsilon^2 \sum_{j=-\infty}^{\infty} |\hat{V}_{p-j,j}|^2\right],$$

using the fact that

$$\mathbb{E}\left[|(\mathcal{Q}^*\hat{W})_p|^2\right] = \varepsilon^2 q_p(\alpha, k)$$

and

$$\left|(\mathcal{Q}^*\hat{V})_p\right|^2 \leq \varepsilon^2 q_p(\alpha, k) \sum_{j=-\infty}^{\infty} |\hat{V}_{p-j,j}|^2\,.$$

We assume the following.

Assumption 1. $\varepsilon^2 \ll \sigma$.

Assumption 1 insures that indeed the instrument errors dominate the approximation error. We remark that below we will assume without loss of generality that $p \geq 1$. We can therefore conclude from (16) that to resolve the pth mode of h, $\hat{h}_p$, we need the following resolving condition to be satisfied:

$$(17) \qquad \left(\frac{\sigma}{\varepsilon}\right)^2 < q_p(\alpha, k),$$

assuming that indeed $\hat{h}_p$ is of order one.

By substituting into definition (14) of q_p the following lower and upper bounds for $c_{n,m}(\alpha, k)$ which follow from Taylor expansion of $c_{n,m}$ with respect to α,

$$(18) \qquad \left(\frac{8\pi(k-1)^2}{4\alpha(k+1)^2}\right)\alpha^{|n|+|m|} \leq |c_{n,m}(\alpha, k)| \leq \left(\frac{8\pi|k-1|}{\alpha(k+1)}\right)\alpha^{|n|+|m|},$$

we immediately find that

$$(19) \qquad \left(\frac{8\pi(k-1)^2}{4(k+1)^2}\right)^2 \leq \frac{q_p(\alpha, k)}{\alpha^{2p-2}\left(\frac{2\alpha^4}{1-\alpha^4}+p-1\right)} \leq \left(\frac{8\pi(k-1)}{(k+1)}\right)^2.$$

We introduce the signal-to-noise ratio, SNR, and the contrast adjusted signal-to-noise ratio SNR_k:

$$(20) \qquad \mathrm{SNR} := \left(\frac{\varepsilon}{\sigma}\right)^2, \qquad \mathrm{SNR}_k := \frac{4\pi^2(k-1)^4}{(k+1)^4}\mathrm{SNR}.$$

Combining (17) and (19), the mode resolving sufficient condition is therefore

$$(21) \qquad \mathrm{SNR}_k^{-1} < \alpha^{2p-2}\left(\frac{2\alpha^4}{1-\alpha^4}+p-1\right).$$

We can see that we have "infinite resolution" in the limit $\alpha \uparrow 1$ in the sense that we can estimate all modes $\hat{h}_p$ in this limit. We correspondingly have the following necessary condition associated with the lower bound in (19):

$$(22) \qquad \widetilde{\mathrm{SNR}}_k^{-1} < \alpha^{2p-2}\left(\frac{2\alpha^4}{1-\alpha^4}+p-1\right)$$

for

$$(23) \qquad \widetilde{\mathrm{SNR}}_k = \frac{64\pi^2(k-1)^2}{(k+1)^2}\mathrm{SNR},$$

which has exactly the same behavior as the sufficient condition (21). Therefore we will now work only with (21).

We can now answer the question: for a fixed SNR and radius α, which modes can be resolved? From the previous analysis the answer is that it is possible to estimate the pth mode up to $p = p(\alpha, \mathrm{SNR}_k)$, where $p(\alpha, \mathrm{SNR}_k)$ is the resolving mode number bound defined by

$$(24) \qquad p(\alpha, \mathrm{SNR}_k) = \sup\left\{p \geq 1 \,\middle|\, \inf_{1 \leq p' \leq p} \alpha^{2p'-2}\left(\frac{2\alpha^4}{1-\alpha^4}+p'-1\right) > \mathrm{SNR}_k^{-1}\right\}.$$

If the set in the sup is empty, then $p(\alpha, \mathrm{SNR}_k) = 0$, which means that estimation is not possible. In Figure 1 we show the maximal mode number $p(\alpha, \mathrm{SNR}_k)$. It is seen that the relative resolution decreases rapidly with "depth" (decreasing radius α). Figure 2 shows the resolution bound, defined by

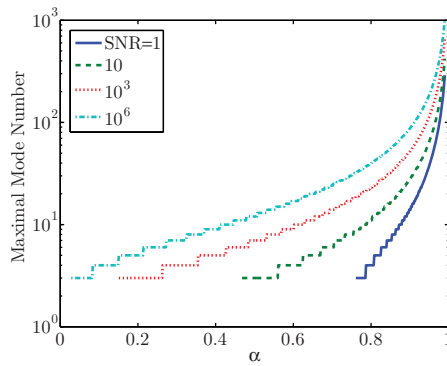$$(25) \qquad \lambda(\alpha, \mathrm{SNR}_k) := 2\pi\frac{\alpha}{p(\alpha, \mathrm{SNR}_k)},$$

FIGURE 1. Maximal mode number $p(\alpha, \mathrm{SNR}_k)$ (see (24)) as a function of radius α and signal-to-noise ratio SNR_k.
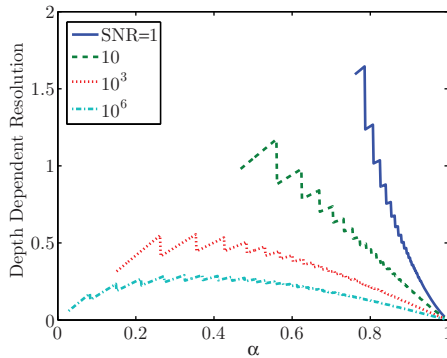

FIGURE 2. Resolution $\lambda(\alpha, \mathrm{SNR}_k)$ (see (25)) as a function of radius α and signal-to-noise ratio SNR_k.

as a function of the radius α and the noise ratio SNR_k. We remark that the resolution measured in this way actually improves for a very small radius due to reduction in scale for fixed p with reduced radius. In fact, for large SNR_k, the function $\alpha \to \lambda(\alpha, \mathrm{SNR}_k)$ is approximately $-4\pi\alpha \ln(\alpha)/\ln(\mathrm{SNR}_k)$ and it has a maximum whose value is $4\pi/(e \ln(\mathrm{SNR}_k))$ for the argument $\alpha = e^{-1}$. We will revisit this observation in the next subsection.

2.3. **Probing in depth with conductivity.** We now revisit the question addressed in the previous subsection by considering the alternative question: for a fixed SNR and mode p, what is the minimal radius α of the inclusion that can be probed? We find from (21) that a resolving condition is $\alpha \geq \alpha^\star(p, \mathrm{SNR}_k)$ where we have defined the "resolving radius" by

$$(26) \qquad\qquad \alpha^\star(p, \mathrm{SNR}_k) = \mathcal{F}_p^{-1}\Big(\frac{1}{\mathrm{SNR}_k}\Big).$$

Here $\mathcal{F}_p^{-1}$ is the inverse of the function $\alpha \to \mathcal{F}_p(\alpha) = \alpha^{2p-2}\big(\frac{2\alpha^4}{1-\alpha^4} + p - 1\big)$ that is increasing and one-to-one from $[0, 1)$ to $[0, \infty)$. The quantity $\alpha^\star(p, \mathrm{SNR}_k)$ has
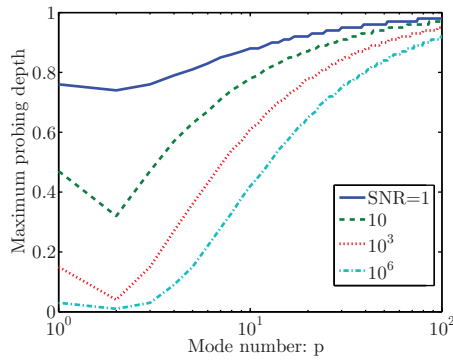
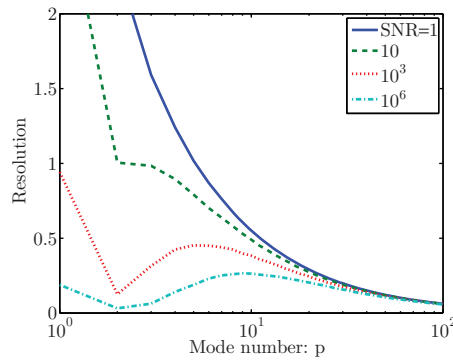FIGURE 3. Resolving radius $\alpha^\star(p, \mathrm{SNR}_k)$ (see (26)) as a function of mode number p and signal-to-noise ratio SNR_k.

FIGURE 4. Resolution $\lambda^\star(p, \mathrm{SNR}_k)$ (see (27)) as a function of mode number p and signal-to-noise ratio SNR_k.

the interpretation of being the smallest radius one can probe for a certain mode number p and signal-to-noise ratio SNR_k. The probing depth is of course limited by SNR_k. By reducing the mode number, one can however probe deeper. We can correspondingly define

$$(27) \qquad \lambda^\star(p, \mathrm{SNR}_k) := \frac{2\pi\alpha^\star(p, \mathrm{SNR}_k)}{p},$$

which has the interpretation of being the resolution at the maximum probing depth. In Figures 3 and 4 respectively we show the resolving radius $\alpha^\star$ and the associated resolution $\lambda^\star$.

In fact, for large SNR_k, $p \mapsto \lambda^\star(p, \mathrm{SNR}_k)$ has a maximum. The argument at the extremal, $p^\star$, satisfies

$$p^\star(\mathrm{SNR}_k) \overset{\mathrm{SNR}_k\uparrow\infty}{\sim} \frac{1}{2}\ln(\mathrm{SNR}_k).$$

We also have

$$\alpha^\star(p^\star(\mathrm{SNR}_k), \mathrm{SNR}_k) \overset{\mathrm{SNR}_k\uparrow\infty}{\sim} e^{-1},$$

which conforms with the behavior seen in Figure 2. We then have the following asymptotic characterization of the resolution:

$$\lambda^{\star}(p^{\star}(\mathrm{SNR}_k), \mathrm{SNR}_k) \overset{\mathrm{SNR}_k \uparrow \infty}{\sim} \frac{4\pi}{e \ln(\mathrm{SNR}_k)}.$$

We conclude that indeed the conductivity is sensitive to noise with a high resolution requiring a very high signal-to-noise ratio.

3. DETECTION WITH HELMHOLTZ DATA

We now change the focus to the wave propagation problem. That is, we consider the case when the data are time-harmonic observations, the solutions of the Helmholtz equation, and the estimation problem analogous to that discussed in the previous section. It has been admitted that on one hand, the resolving power of waves is of order half the wavelength, and on the other hand, stability increases with frequency. Here, we show that the resolution and stability analysis heavily depends on the regime we are considering. The estimates of the resolving power (or the resolution measure) in terms of the SNR of the measurements are completely different in the high-frequency regime from those in the low-frequency regime. Moreover, we clarify the link between conductivity and low-frequency imaging. High SNR is needed for imaging in both cases. In the high-frequency regime, the estimation of the resolving power is relatively insensitive to noise.

3.1. **Differential measurements.** The measurements are taken on a circle of unit radius in a non-dimensionalized setting. The domain of interest and the perturbation domain is as before characterized by (1) and (2). Following [2] we model the estimation problem below. Suppose first that the inclusion D_ε is illuminated by an array of N elements $\{\boldsymbol{y}_1, \ldots, \boldsymbol{y}_N\}$. In polar coordinates the points of the transmitter array are $\boldsymbol{y}_n = (\cos\theta_n, \sin\theta_n)$. In this case, the field perturbed in the presence of the inclusion is the solution $u(\cdot, \boldsymbol{y}_m)$ to the following transmission problem:

$$(28) \quad \begin{cases} \Delta u + \dfrac{\omega^2}{c_0^2} u = -\delta_{\boldsymbol{y}_m}, & \text{in } \mathbb{R}^2 \setminus \overline{D_\varepsilon}, \\[2mm] \Delta u + \dfrac{\omega^2}{c^2} u = 0, & \text{in } D_\varepsilon, \\[2mm] u\big|_+ - u\big|_- = 0, & \text{on } \partial D_\varepsilon, \\[2mm] \dfrac{\partial u}{\partial \nu}\Big|_+ - \dfrac{\partial u}{\partial \nu}\Big|_- = 0, & \text{on } \partial D_\varepsilon, \\[2mm] u \text{ satisfies the outgoing radiation condition,} \end{cases}$$

where ω/c_0 and ω/c are the wavenumbers associated with the free space and the inclusion respectively. Here, D_ε is defined by (3) and $D_{\varepsilon=0} = D$ given by (2).

Suppose also that the receiver array used to detect the inclusion coincides with the transmitter array. The data consists of the multi-static response (MSR) matrix $\mathbf{A} = (A_{n,m})_{n,m=1,\ldots,N}$ which describes the transmit-receive process performed by this array. In the presence of the inclusion the scattered field induced on the nth receiving element, $\boldsymbol{y}_n$, from the scattering of an incident wave generated at $\boldsymbol{y}_m$ can be expressed as follows:

$$(29) \quad A_{n,m} = u(\boldsymbol{y}_n, \boldsymbol{y}_m) - \Gamma^{q_0}(\boldsymbol{y}_n - \boldsymbol{y}_m).$$

Here $q_0 = \omega/c_0$ is the homogeneous wavenumber, Γ^{q_0} is the associated free space Green's function,

$$(30) \qquad \Gamma^{q_0}(\boldsymbol{x}) = \frac{i}{4} H_0^{(1)}\big(q_0|\boldsymbol{x}|\big) \overset{q_0|\boldsymbol{x}|\gg 1}{\simeq} \frac{e^{i\pi/4}}{2\sqrt{2\pi q_0|\boldsymbol{x}|}} e^{iq_0|\boldsymbol{x}|},$$

and $H_0^{(1)}$ is the Hankel function of the first kind of order zero.

The problem we consider is how to image the inclusion D_ε from the MSR matrix. We assume that the target is extended; i.e., its characteristic size is much larger than half the wavelength π/q_0.

Let us define the contrast parameter

$$(31) \qquad \mathcal{C} = \frac{c_0^2}{c^2} - 1.$$

As shown in [2] (see also [18, 19, 27]) the response matrix is given asymptotically when $c \sim c_0$ by

$$(32) \qquad A_{m,n}[D] = \frac{iq_0\mathcal{C}}{8\pi} \int_D e^{iq_0[|\boldsymbol{y}_n - \boldsymbol{x}| + |\boldsymbol{y}_m - \boldsymbol{x}|]} d\boldsymbol{x}.$$

Using the Taylor series expansion

$$(33) \qquad |\boldsymbol{y}_n - \boldsymbol{x}| = |\boldsymbol{y}_n| - \frac{\boldsymbol{y}_n \cdot \boldsymbol{x}}{|\boldsymbol{y}_n|} + O\Big(\frac{|\boldsymbol{x}|^2}{|\boldsymbol{y}_n|}\Big),$$

we find that, in polar coordinates $\boldsymbol{x} = (r\cos\theta, r\sin\theta)$,

$$(34) \qquad A_{m,n}[D] = e^{i(2q_0 + \pi/2)} \frac{q_0\mathcal{C}}{8\pi} \int_0^{2\pi} d\theta \int_0^\alpha r\,dr\, e^{-iq_0 r[\cos(\theta - \theta_m) + \cos(\theta - \theta_n)]},$$

which is valid if the Rayleigh distance $q_0\mathrm{diam}^2(D)$ is smaller than the distance from the target D to the array (this is the Fraunhofer regime). Thus, we make the following assumption:

Assumption 2. $\alpha^2 q_0 \ll 1$.

Similarly, we have for the case of measurements from the perturbed domain

$$(35) \quad A_{m,n}[D_\varepsilon] = e^{i(2q_0 + \pi/2)} \frac{q_0\mathcal{C}}{8\pi} \int_0^{2\pi} d\theta \int_0^{\alpha + \varepsilon h(\theta)} r\,dr\, e^{-iq_0 r[\cos(\theta - \theta_m) + \cos(\theta - \theta_n)]}.$$

Expansions (32) and (35) are known as the Born approximations.

In the continuum approximation the response matrix of the unperturbed domain then corresponds to the operator whose kernel is

$$(36) \qquad \mathcal{A}[D](\theta_1, \theta_2) = \frac{q_0\mathcal{C}}{8\pi} \int_0^{2\pi} d\theta \int_0^\alpha r\,dr\, e^{-iq_0 r[\cos(\theta - \theta_1) + \cos(\theta - \theta_2)]}.$$

In fact,

$$A_{m,n}[D] = e^{i(2q_0 + \pi/2)} \int_0^{2\pi} \int_0^{2\pi} \mathcal{A}[D](\theta_1, \theta_2)\, \delta(\theta_1 - \theta_m)\delta(\theta_2 - \theta_n)\, d\theta_1 d\theta_2,$$

where δ is the Dirac delta function. The kernel of the operator corresponding to the perturbed domain has a similar expression with $\alpha + \varepsilon h(\theta)$ instead of α. From the asymptotic expansion of $A_{m,n}[D_\varepsilon]$ in (35) as $\varepsilon \to 0$ [2], it follows that the kernel associated with differential measurements can be written as

$$(37) \qquad \mathcal{H}[D](\theta_1, \theta_2) = \frac{q_0\mathcal{C}\alpha\varepsilon}{8\pi} \int_0^{2\pi} d\theta\, e^{-iq_0\alpha[\cos(\theta - \theta_1) + \cos(\theta - \theta_2)]} h(\theta).$$

It is convenient to express the data in the continuum approximation and in the Fourier domain as the singular vectors of the kernel which indeed constitute the Fourier basis. This moreover corresponds to the measurement configuration of the conductivity case discussed in the previous section. In the Fourier domain, the observations are

$$(38) \qquad \hat{b}_{n,m} = \frac{1}{(2\pi)^2} \int_0^{2\pi} \int_0^{2\pi} \mathcal{H}[D](\theta_1, \theta_2) e^{-i(n\theta_1 + m\theta_2)} d\theta_1 d\theta_2 \,.$$

Using Neumann's formula [16, Formula 7.7.2(11)], it follows from (38) that $\hat{b}_{n,m}$ are given by

$$(39) \qquad \hat{b}_{n,m} = \frac{\varepsilon q_0 \mathcal{C} \alpha}{4} J_n(q_0 \alpha) J_m(q_0 \alpha) i^{-(n+m)} \hat{h}_{n+m} \,,$$

where the J_n's are the Bessel functions of the first kind. The coefficients $\hat{b}_{n,m}$ are the analogue of $\hat{a}_{n,m}$ for the conductivity case. The analogue of (9) then becomes

$$(40) \qquad \hat{b}_{n,m} = (\mathcal{R}\hat{h})_{n,m} \,, \qquad (\mathcal{R}\hat{h})_{n,m} = \frac{\varepsilon q_0 \mathcal{C} \alpha}{4} J_n(q_0 \alpha) J_m(q_0 \alpha) i^{-(n+m)} \hat{h}_{n+m} \,.$$

If we incorporate instrument noise and again assume that the effect of approximation error is relatively small, then we can write

$$(41) \qquad \hat{b}_{n,m}^{\text{meas}} = \hat{b}_{n,m} + \sigma \hat{W}_{n,m} \,,$$

with $\hat{W}_{n,m}$ again being modeled as standard and independent circularly symmetric Gaussian entries.

We then get the least squares estimate,

$$
\begin{aligned}
(42) \qquad \hat{h}_{\text{est},p} &= \hat{h}_p + \sigma \left((\mathcal{R}^* \mathcal{R})^{-1} \mathcal{R}^* \hat{W} \right)_p \\
&= \hat{h}_p + \frac{4\sigma}{\varepsilon q_0 \mathcal{C} \alpha} \frac{\sum_{l=-\infty}^{\infty} J_l(q_0 \alpha) J_{p-l}(q_0 \alpha) i^p \hat{W}_{l,p-l}}{\sum_{l=-\infty}^{\infty} J_l^2(q_0 \alpha) J_{p-l}^2(q_0 \alpha)} \,,
\end{aligned}
$$

which shows that the estimation is unbiased with the variance

$$
\begin{aligned}
\text{Var}(\hat{h}_{\text{est},p}) &= \mathbb{E}\left[\left| \hat{h}_{\text{est},p} - \hat{h}_p \right|^2 \right] = \left(\frac{4\sigma}{\varepsilon q_0 \mathcal{C} \alpha} \right)^2 \frac{1}{\sum_{l=-\infty}^{\infty} J_l^2(q_0 \alpha) J_{p-l}^2(q_0 \alpha)} \\
(43) \qquad &= \left(\frac{4\sigma}{\varepsilon q_0 \mathcal{C} \alpha} \right)^2 \frac{2\pi}{\int_0^{2\pi} J_p^2(2q_0 \alpha \cos\theta) d\theta} \,.
\end{aligned}
$$

Here we have used the identity

$$(44) \qquad \sum_{l=-\infty}^{\infty} J_l^2(q_0 \alpha) J_{p-l}^2(q_0 \alpha) = \frac{1}{2\pi} \int_0^{2\pi} J_p^2(2q_0 \alpha \cos\theta) d\theta \,,$$

which follows from Neumann's formula and Parseval's formula.

We consider in the next two subsections the high- and low-frequency regimes.

3.2. **High-frequency regime.** We consider the high-frequency regime defined by:

Assumption 3. $q_0 \alpha \gg 1$.

We remark that Assumptions 2 and 3 imply $\alpha \ll 1$ and $q_0 \gg 1$. In this asymptotic framework, when p is smaller than $2q_0\alpha$, then we have [26, Eq. 4]

$$\frac{1}{2\pi} \int_0^{2\pi} J_p^2(2q_0\alpha\cos\theta)d\theta = \frac{1}{\pi^2 q_0\alpha}\Big[\log q_0\alpha + 5\ln 2 + \gamma - 2\big(1 + \frac{1}{3} + \cdots + \frac{1}{2p-1}\big)$$

$$(45) \qquad\qquad\qquad\qquad\qquad\qquad\qquad\qquad +O\big((q_0\alpha)^{-1/2}\big)\Big],$$

where γ is the Euler's constant, while when p is larger than $2q_0\alpha$, the integral is exponentially close to zero [1, Eq. 9.3.2]:

$$(46) \qquad\qquad \frac{1}{2\pi} \int_0^{2\pi} J_p^2(2q_0\alpha\cos\theta)d\theta \sim \exp\Big[-4q_0\alpha R\big(\frac{p}{2q_0\alpha}\big)\Big],$$

with $R(s) = s\big[\cosh^{-1}(s) - \tanh\big(\cosh^{-1}(s)\big)\big]$ and $\cosh^{-1}$ is the inverse hyperbolic cosine.

We introduce the signal-to-noise ratio SNR and the contrast adjusted signal-to-noise ratio $\mathrm{SNR}_{\mathcal{C}}$:

$$(47) \qquad\qquad \mathrm{SNR} = \Big(\frac{\varepsilon}{\sigma}\Big)^2, \qquad \mathrm{SNR}_{\mathcal{C}} = \mathcal{C}^2\mathrm{SNR}.$$

The stability condition that allows for the estimation of the pth mode is

$$(48) \qquad\qquad \mathrm{Var}(\hat{h}_{\mathrm{est},p}) < 1,$$

with $\mathrm{Var}(\hat{h}_{\mathrm{est},p})$ given by (43). For $p < 2q_0\alpha$, this condition reads

$$(49) \qquad\qquad \mathrm{SNR}_{\mathcal{C}}^{-1} < \frac{q_0\alpha\log(q_0\alpha)}{(4\pi)^2}.$$

For $p > 2q_0\alpha$ the condition (48) means that $\mathrm{SNR}_{\mathcal{C}}^{-1}$ should be exponentially large in $q_0\alpha$. Therefore we need $p < 2q_0\alpha$, otherwise the signal is exponentially small and the constraint on the signal-to-noise ratio is prohibitive. This corresponds to the "global" resolution constraint:

$$(50) \qquad\qquad p \leq p(\alpha), \qquad \frac{2\pi\alpha}{p(\alpha)} = \frac{\lambda_0}{2},$$

where $\lambda_0 = 2\pi/q_0$ is the homogeneous wavelength. Thus, this constraint limits the resolution to half the wavelength.

In order to estimate the coefficients $\hat{h}_p$ for all $p \leq 2q_0\alpha$, we need (49) to be satisfied. Note that a large parameter $q_0\alpha$ actually allows for the estimation of the coefficients $\hat{h}_p$ for a small $\mathrm{SNR}_{\mathcal{C}}$ since the high-frequency q_0 amplifies the returns as shown in (37). This shows that in this high-frequency regime the estimation is relatively insensitive to noise. From (49) we have for the probing constraint

$$(51) \qquad \alpha \geq \alpha^\star(\mathrm{SNR}_{\mathcal{C}}), \qquad \alpha^\star(\mathrm{SNR}_{\mathcal{C}}) = \frac{\lambda_0}{2\pi}\mathcal{F}^{-1}\big((4\pi)^2\mathrm{SNR}_{\mathcal{C}}^{-1}\big),$$

where $\mathcal{F}(x) = x\log x$ is an increasing one-to-one function from $[1, \infty)$ to $[0, \infty)$. The radius $\alpha^\star$ is the minimal radius of the inclusion that can be probed and estimated with a signal-to-noise ratio $\mathrm{SNR}_{\mathcal{C}}$ in the high-frequency regime. In Figure 5 we show the relative minimal resolving radius $\alpha^\star/\lambda_0$ as a function of $\mathrm{SNR}_{\mathcal{C}}$. We remark that Assumption 3 means that $2\pi\alpha/\lambda_0 \gg 1$.
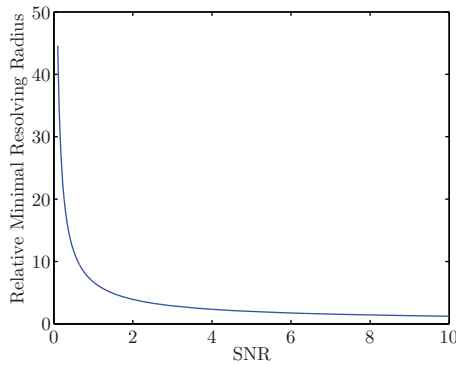
FIGURE 5. Relative minimal radius $\alpha^\star(\mathrm{SNR}_{\mathcal{C}})/\lambda_0$ (see (51)) as a function of $\mathrm{SNR}_{\mathcal{C}}$ in the high-frequency regime.

3.3. **Low-frequency regime.** We consider the low-frequency regime defined by:

Assumption 4. $q_0\alpha \ll 1$.

In the asymptotic framework when $q_0\alpha \ll 1$, using the fact that $J_p(z) \overset{z\to 0}{\sim} (z/2)^p/p!$, we have

$$(52) \qquad \frac{1}{2\pi}\int_0^{2\pi} J_p^2(2q_0\alpha\cos\theta)d\theta \sim (q_0\alpha)^{2p}\mathcal{H}(p),$$

with

$$(53) \qquad \mathcal{H}(p) = \frac{1}{2\pi(p!)^2}\int_0^{2\pi}\cos^{2p}(\theta)d\theta = \frac{1}{4}\frac{(2p)!}{2^{2p}(p!)^4}.$$

We then get (as in (48)) the stability condition that allows for the estimation of the pth mode:

$$(54) \qquad \mathrm{SNR}_{\mathcal{C}}^{-1} < \frac{(q_0\alpha)^{2p+2}\mathcal{H}(p)}{4} = \Big(\frac{2\pi\alpha}{\lambda_0}\Big)^{2p+2}\frac{\mathcal{H}(p)}{4}.$$

Note the qualitatively different dependence on the mode number in the high- and low-frequency regimes (compare with (49)). We can now answer the question: for a fixed $\mathrm{SNR}_{\mathcal{C}}$ and α, which modes can be resolved? The answer is that it is possible to estimate modes up to $p = p(\alpha/\lambda_0, \mathrm{SNR}_{\mathcal{C}})$ with

$$(55) \qquad p(\alpha/\lambda_0, \mathrm{SNR}_{\mathcal{C}}) = \sup\left\{p \geq 1 \,\Big|\, \inf_{1\leq p'\leq p}\Big(\frac{2\pi\alpha}{\lambda_0}\Big)^{2p'+2}\frac{\mathcal{H}(p')}{4} > \mathrm{SNR}_{\mathcal{C}}^{-1}\right\}.$$

We plot in Figure 6 the maximal mode number $p(\alpha/\lambda_0, \mathrm{SNR}_{\mathcal{C}})$ as a function of the relative radius α/λ_0 and signal-to-noise ratio $\mathrm{SNR}_{\mathcal{C}}$. We remark that Assumption 4 means that $2\pi\alpha/\lambda_0 \ll 1$. Note that a high signal-to-noise ratio is needed in this low-frequency regime even to get estimates of relatively low modes. Figure 7 shows the resolution bound as defined by (25):

$$(56) \qquad \frac{\lambda(\alpha/\lambda_0, \mathrm{SNR}_{\mathcal{C}})}{\lambda_0} = 2\pi\frac{\alpha/\lambda_0}{p(\alpha/\lambda_0, \mathrm{SNR}_{\mathcal{C}})},$$

with $p(\alpha/\lambda_0, \mathrm{SNR}_{\mathcal{C}})$ given by (55).
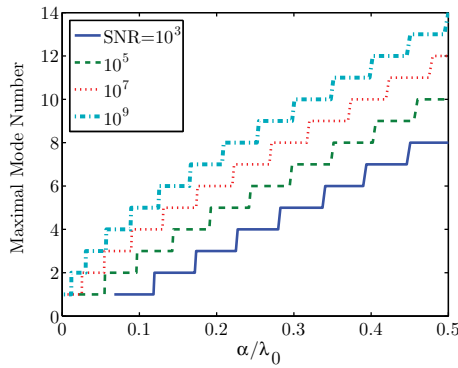
FIGURE 6. Maximal mode number $p(\alpha/\lambda_0, \mathrm{SNR}_{\mathcal{C}})$ (see (55)) as a function of relative radius α/λ_0 and $\mathrm{SNR}_{\mathcal{C}}$ in the low-frequency regime.
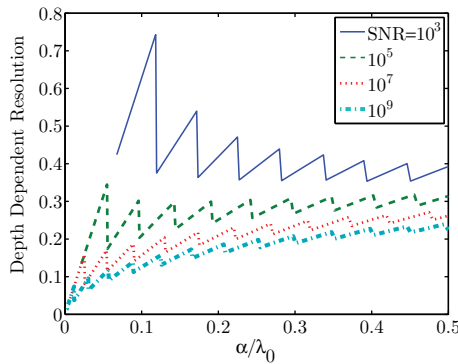

FIGURE 7. Relative resolution $\lambda(\alpha/\lambda_0, \mathrm{SNR}_{\mathcal{C}})/\lambda_0$ (see (56)) as a function of relative radius α/λ_0 and $\mathrm{SNR}_{\mathcal{C}}$ in the low-frequency regime.

In terms of the radial dependence we can contrast (54) with the corresponding condition in (21). The low-frequency limit is very sensitive to the noise conforming with the discussion of the conductivity case in the previous section. From (54) we have the probing constraint

$$(57) \qquad \alpha \geq \alpha^{\star}(p, \mathrm{SNR}_{\mathcal{C}}), \qquad \alpha^{\star}(p, \mathrm{SNR}_{\mathcal{C}}) = \frac{\lambda_0}{2\pi}\Big(\frac{4}{\mathcal{H}(p)\mathrm{SNR}_{\mathcal{C}}}\Big)^{1/(2p+2)},$$

which is the low-frequency version of (51). This answers the question: for the mode number p that we want to resolve and a given signal-to-noise ratio $\mathrm{SNR}_{\mathcal{C}}$, what is the minimum radius $\alpha^{\star}$ that we can probe? We plot the relative minimal radius $\alpha^{\star}/\lambda_0$ in Figure 8.

We can next associate the relative minimum radius with the resolution measure $\lambda^{\star}(p, \mathrm{SNR}_{\mathcal{C}}) = 2\pi\alpha^{\star}(p, \mathrm{SNR}_{\mathcal{C}})/p$. Thus, we introduce the p- and SNR-dependent
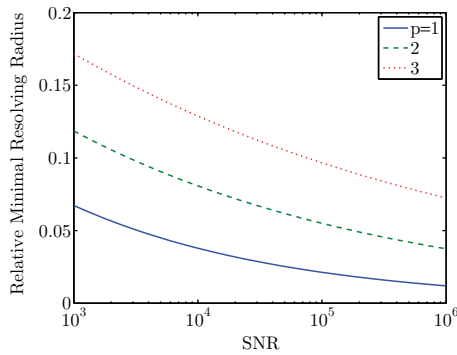
FIGURE 8. Relative minimal radius $\alpha^\star(p, \mathrm{SNR}_\mathcal{C})/\lambda_0$ (see (57)) as a function of $\mathrm{SNR}_\mathcal{C}$ and mode number p in the low-frequency regime.
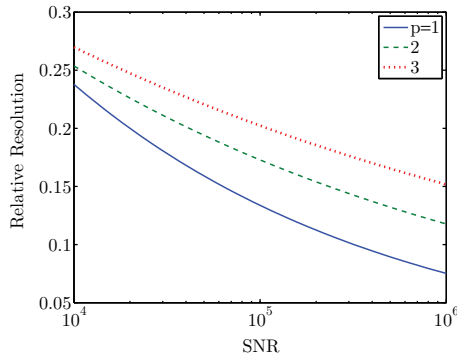

FIGURE 9. Relative resolution measure $\lambda^\star(p, \mathrm{SNR}_\mathcal{C})/\lambda_0$ in the low-frequency regime (see (58)) as a function of $\mathrm{SNR}_\mathcal{C}$ and mode number p.

resolution constraint by

$$(58) \qquad \lambda^\star(p, \mathrm{SNR}_\mathcal{C}) = \frac{\lambda_0}{p}\Big(\frac{4}{\mathcal{H}(p)\mathrm{SNR}_\mathcal{C}}\Big)^{1/(2p+2)}.$$

A small $\lambda^\star$ corresponds to a good resolution. Using Stirling's formula, it follows from (58) that

$$(59) \qquad \lambda^\star(p, \mathrm{SNR}_\mathcal{C}) \overset{p\to\infty}{\sim} \frac{\lambda_0}{e}.$$

Therefore, in the low-frequency regime, there is a saturation effect for the resolution. In Figure 9, we plot the resolution measure $\lambda^\star(p, \mathrm{SNR}_\mathcal{C})/\lambda_0$. Figure 9 shows that, in this low-frequency regime, a relatively high SNR is needed. Moreover, with a very high signal-to-noise ratio the relative resolution can then be very high. It in fact increases with the SNR but saturates for high modes.

References

[1] M. Abramowitz and I. Stegun (editors), *Handbook of Mathematical Functions*, National Bureau of Standards, Washington, D.C., 1964.

[2] H. Ammari, J. Garnier, H. Kang, M. Lim, and K. Sølna, Multistatic imaging of extended targets, SIAM J. Imaging Science, 5 (2012), 564–600. MR2971173

[3] H. Ammari, J. Garnier, and K. Sølna, Limited view resolving power of conductivity imaging from boundary measurements, submitted.

[4] H. Ammari, H. Kang, and H. Lee, *Layer Potential Techniques in Spectral Analysis*, Mathematical Surveys and Monographs, Vol. 153, Amer. Math. Soc., Providence, RI, 2009. MR2488135 (2010j:47062)

[5] H. Ammari, H. Kang, M. Lim, and H. Zribi, Conductivity interface problems. Part I: Small perturbations of an interface, Trans. Amer. Math. Soc., 362 (2010), 2435–2449. MR2584606

[6] G. Bao, Y. Chen, and F. Ma, Regularity and stability for the scattering map of a linearized inverse medium problem, J. Math. Anal. Appl., 247 (2000), 255–271. MR1766937 (2001f:35423)

[7] E. Beretta and E. Francini, Asymptotic formulas for perturbations in the electromagnetic fields due to the presence of thin inhomogeneities, in *Inverse problems: theory and applications*, Contemp. Math., 333, Amer. Math. Soc., Providence, RI, 2003. MR2032006 (2005a:35263)

[8] M. Bertero, P. Boccacci, and M. Piana, Resolution and super-resolution in inverse diffraction, in *Inverse Problems of Wave Propagation and Diffraction*, Lecture Notes in Physics, Vol. 486, 1–17, Springer, Berlin, 1997. MR1601171 (98j:65073)

[9] L. Borcea, Electrical impedance tomography, Inverse Problems 18 (2002), R99–R136. MR1955896

[10] L. Borcea, G. Papanicolaou, and F. G. Vasquez, Edge illumination and imaging of extended reflectors, SIAM J. Imaging Sci., 1 (2008), 75–114. MR2475826 (2010a:15028)

[11] M. Born and E. Wolf, *Principles of Optics*, Cambridge University Press, Cambridge, 1999.

[12] D. C. Dobson, Estimates on resolution and stabilization for the linearized inverse conductivity problem, Inverse Problems, 8 (1992), 71–81. MR1153128 (92m:35269)

[13] D. C. Dobson and F. Santosa, Resolution and stability analysis of an inverse problem in electrical impedance tomography: dependence on the input current patterns, SIAM J. Appl. Math., 54 (1994), 1542–1560. MR1301272 (95g:35212)

[14] G. Derveaux, G. Papanicolaou, and C. Tsogka, Resolution and denoising in near-field imaging, Inverse Problems, 22 (2006), 1437–1456. MR2249472 (2007b:76110)

[15] H.W. Engl, M. Hanke, and A Neubauer, *Regularization of Inverse Problems*, Kluwer, Dordrecht, 1996. MR1408680 (97k:65145)

[16] A. Erdélyi, W. Magnus, F. Oberhettinger, and F. G. Tricomi (editors), *Higher Transcendental Functions, Vol. II*, McGraw-Hill, New York, 1953. MR0058756 (15:419i)

[17] B. Harrach and J. K. Seo, Exact shape-reconstruction by one-step linearization in electrical impedance tomography, SIAM J. Math. Anal., 42 (2010), 1505–1518. MR2679585 (2011h:35316)

[18] S. Hou, K. Sølna, and H. Zhao, A direct imaging algorithm for extended targets, Inverse Problems, 22 (2006), 1151–1178. MR2249458 (2007b:78009)

[19] S. Hou, K. Sølna, and H. Zhao, Imaging of location and geometry for extended targets using the response matrix, J. Comput. Phys., 199 (2004), 317–338. MR2081006 (2005k:78016)

[20] D. Isaacson and E. L. Isaacson, Comment on A.-P. Calderón paper: "On an inverse boundary value problem", Math. Comp., 52 (1989), 553–559. MR962208 (90f:35201)

[21] V. Isakov, Increased stability in the Cauchy problem for some elliptic equations, in *Instability in Models Connected with Fluid Flows. I*, C. Bardos and A. Fursikov, eds., International Math. Series, Vol. 6, 339–362, Springer, 2008. MR2459261 (2009g:35038)

[22] P. Kearey, M. Brooks, and I. Hill, *An Introduction to Geophysical Exploration*, 3rd edition, Blackwell Science, Oxford, 2002.

[23] N. Mandache, Exponential instability in an inverse problem for the Schrödinger equation, Inverse Problems, 17 (2001), 1435–1444. MR1862200 (2002h:35339)

[24] S. Nagayasu, G. Uhlmann, and J.-N. Wang, Depth dependent stability estimates in electrical impedance tomography, Inverse Problems, 25 (2009), 075001. MR2519853 (2010g:65195)

[25] D. Slepian, Some comments on Fourier analysis, uncertainty and modeling, SIAM Review, 25 (1983), 379–393. MR710468 (84i:94016)

[26] R. Wong, Asymptotic expansion of $\int_0^{\pi/2} J_\nu^2(\lambda\cos\theta)d\theta$, Math. Comput., 50 (1988), 229–234. MR917830 (89g:41022)
[27] H. Zhao, Analysis of the response matrix for an extended target, SIAM J. Appl. Math., 64 (2004), 725–745. MR2068119 (2005a:74050)

DEPARTMENT OF MATHEMATICS AND APPLICATIONS, ÉCOLE NORMALE SUPÉRIEURE, 45 RUE D'ULM, 75005 PARIS, FRANCE
  E-mail address: `habib.ammari@ens.fr`

LABORATOIRE DE PROBABILITÉS ET MODÈLES ALÉATOIRES AND LABORATOIRE JACQUES-LOUIS LIONS, UNIVERSITÉ PARIS VII, 75205 PARIS CEDEX 13, FRANCE
  E-mail address: `garnier@math.jussieu.fr`

DEPARTMENT OF MATHEMATICS, UNIVERSITY OF CALIFORNIA, IRVINE, CALIFORNIA 92697
  E-mail address: `ksolna@math.uci.edu`